Available online at www.sciencedirect.com
ScienceDirect
Magnetic Resonance Imaging 25 (2007) 47–56
MAGNETIC RESONANCE IMAGING

Detecting functional connectivity in the resting brain: a comparison between ICA and CCA

Liangsuo Ma[a,*], Binquan Wang[b], Xiying Chen[a], Jinhu Xiong[a]

[a]*Department of Radiology, University of Iowa, Iowa City, IA 52242, USA*
[b]*Research Imaging Center, University of Texas Health Science Center, San Antonio, TX 78284, USA*

Received 5 May 2006; accepted 12 September 2006

Abstract

Independent component analysis (ICA) and cross-correlation analysis (CCA) are general tools for detecting resting-state functional connectivity. In this study, we jointly evaluated these two approaches based on simulated data and in vivo functional magnetic resonance imaging data acquired from 10 resting healthy subjects. The influence of the number of independent components (maps) on the results of ICA was investigated. The influence of the selection of the seeds on the results of CCA was also examined. Our results reveal that significant differences between these two approaches exist. The performance of ICA is superior as compared with that of CCA; in addition, the performance of ICA is not significantly affected by structured noise over a relatively large range. The results of ICA could be affected by the number of independent components if this number is too small, however. Converting the spatially independent maps of ICA into *z* maps for thresholding tends to overestimate the false-positive rate. However, the overestimation is not very severe and may be acceptable in most cases. The results of CCA are dependent on seeds location. Seeds selected based on different criteria will significantly affect connectivity maps.

Keywords: fMRI; Neuroimaging; Functional connectivity; Cross-correlation analysis; ICA

1. Introduction

Resting-state functional magnetic resonance imaging (fMRI) is instrumental for investigating the functional connectivity of the human brain. It has been successfully applied to study motor [1–3], visual [4], auditory [5] and language [6] systems for healthy subjects and patients [7–9]. Most resting-state fMRI processings performed so far used cross-correlation analysis (CCA), in which neuronal activations are detected by evaluating the correlation between the time course of each voxel and a reference function. Although often determined based on experimental designs (i.e., stimulation presentations) and brain hemodynamics for task-induced activation studies, the reference function is much more difficult to be constructed for resting-sate fMRI studies due to the very limited prior knowledge. A common practice is then using the averaged time course of a preselected brain region as the reference function. Thus, the shape, size and location of the seeds will affect the reference function and, consequently, the outcomes of the resulting connectivity map. Currently, the seeds region is commonly determined based on either brain anatomies [10,11] or additional functional activation studies [2]. The consistency of connectivity maps reported by different laboratories may be deteriorated with the use of different seed selection methods. In the meantime, the seeds approach may also amplify intersubject variability in resting-state connectivity maps because of intersubject variability in anatomy and variability in anatomy–function correspondence.

An alternative to CCA, independent component analysis (ICA) is an exploratory method and requires no reference function or predefined seed [12–16]. It is a statistical technique that drives a set of measurement data into a number of independent signals. First introduced into neuroimaging data processing by McKeown et al. [15] to determine the spatial and temporal characteristics of task-induced brain activations, ICA gradually became one of the widely used techniques for fMRI data analyses. It assumes that all components of brain activation signals are spatially

* Corresponding author. Tel.: +1 319 356 4553; fax: +1 319 356 2220.
E-mail address: liangsuo-ma@uiowa.edu (L. Ma).

0730-725X/$ – see front matter © 2007 Elsevier Inc. All rights reserved.
doi:10.1016/j.mri.2006.09.032

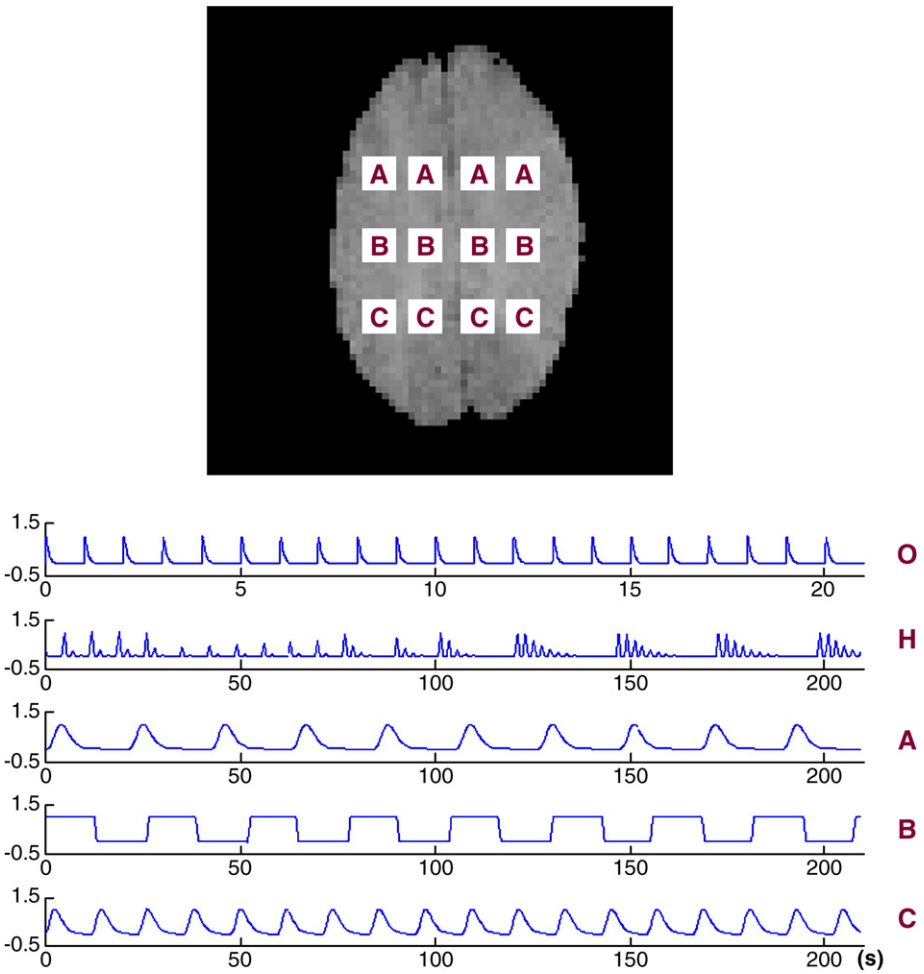

Fig. 1. EPI scan image, selected regions of interest and simulated fMRI signals. Signals O (1.10±0.10 Hz), A (0.05 Hz) and C (0.08 Hz) are series of gamma variate functions simulating heartbeat signal, event-related design fMRI signal and resting-state hemodynamics, respectively. Signal B (0.04 Hz) is a square wave simulating a block-design fMRI signal. Signal H (0.11 Hz) is the simulated aliased cardiac signal by resampling Signal O.

and/or temporally independent. By maximizing spatial independence or temporal independence, ICA can be classified as spatial ICA (sICA) [15,17] or as temporal ICA (tICA) [17,18]. Emphasizing on different aspects (spatial or temporal) of brain activation, sICA and tICA may report different results. The similarities and differences of sICA and tICA have been evaluated and discussed by Calhoun et al. [17]. When both spatial independence assumption and temporal independence assumption are met, sICA and tICA report similar results [17]. In addition to assessing the performances of different ICA techniques, studies have also evaluated the merits of ICA relative to CCA [19] and the temporal clustering technique [20] for task-induced activation.

Requiring no prior knowledge regarding spatial or temporal patterns of brain response, ICA should be best suitable for analyzing resting-state fMRI data, which have very limited prior knowledge of activation. The first application of ICA in resting-state fMRI data analysis was reported by Kiviniemi et al. [7] in 2003. Subsequent applications showed that ICA is able to detect functional connectivity in both primary (motor, visual and somatosensory) and higher-order [21–23] brain regions. It has also been demonstrated that ICA is capable of formulating the same kind of functional connectivity (e.g., motor systems) into a single map [22].

Although CCA and ICA are capable of resting-state analyses, each has its distinctive advantages and pitfalls. The major shortcoming of CCA is the dependence of the resulting connectivity maps on the selection of the seeds region. The major drawbacks of ICA are that (1) it is often difficult to extract true activation maps from a large number of independent components (ICs) and (2) it is often difficult to determine threshold. How to determine the optimal number of independent maps and how to determine the optimal threshold have become open questions. It therefore should be valuable to assess the effects of the number of ICs, threshold and seeds selection on the resulting connectivity maps and to jointly evaluate the performances of ICA and CCA for resting-state fMRI data analyses. To our best knowledge, such evaluations have not been performed. In this study, we first evaluated the effects of seeds selection on

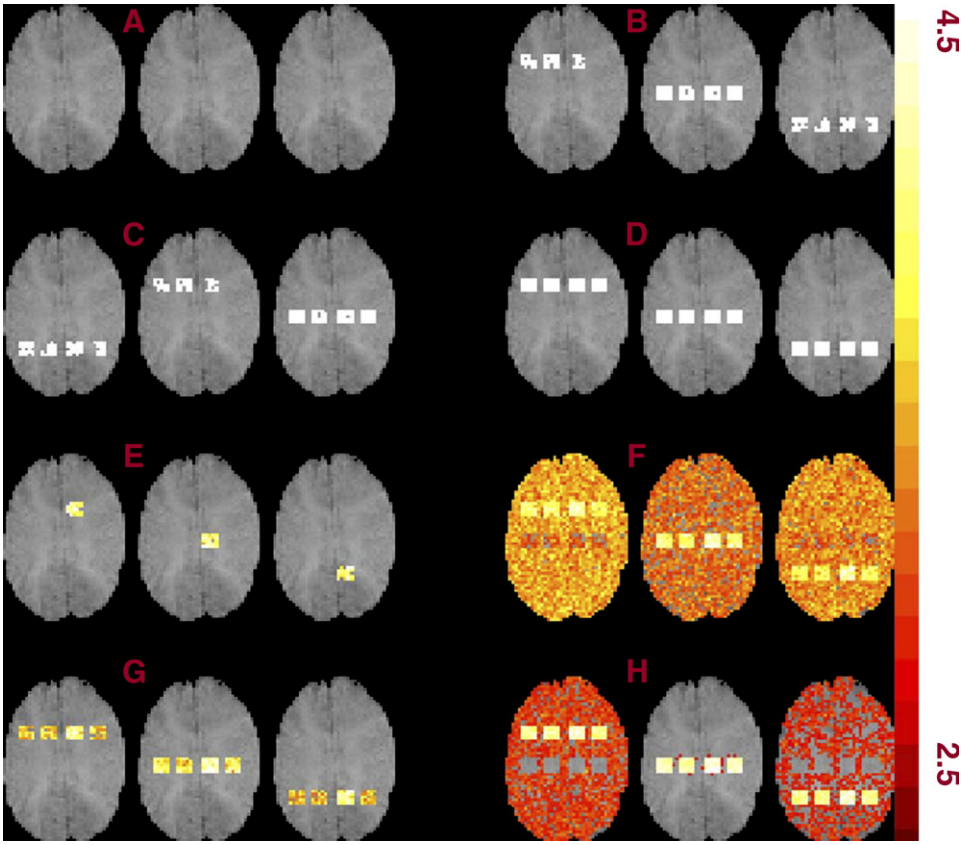

Fig. 2. Functional connectivity networks detected by ICA and CCA under different CNRs and different random-to-structured noise weightings (K). (A) ICA results with CNR = 0.5 and K = 2.0. (B) ICA results with CNR = 0.5 and K = 0.5. (C) ICA results with CNR = 1.0 and K = 2.0. (D) ICA results with CNR = 1.0 and K = 0.5. (E) CCA results with CNR = 0.5 and K = 2.0. (F) CCA results with CNR = 0.5 and K = 0.5. (G) CCA results with CNR = 1.0 and K = 2.0. (H) CCA results with CNR = 1.0 and K = 0.5. Note that the three functional connectivity network maps of ICA were detected simultaneously and that the three maps of CCA were detected by using three seeds in three runs (seeded on Signals A, B and C).

CCA connectivity maps; we then investigated the influences of the number of ICs and threshold on the results of ICA. Finally, we evaluated the relative merits of CCA and ICA based on simulated data and real MRI data.

2. Materials and methods

2.1. Simulation

Simulated data were used to investigate the influences of noise level and threshold on the performances of ICA and CCA. The effect of the number of independent maps on the ICA results was also studied. The echo-planar imaging (EPI) scans and the simulated signals used in this section are shown in Fig. 1. A volume of three-slice EPI scans (each slice has 72×72 voxels) was replicated 300 times to simulate 300 time points of noise-free fMRI data. Three simulated signals (Signals A–C) have been constructed to represent event-related brain hemodynamics (Signal A), block-design brain hemodynamics (Signal B) and resting-state brain hemodynamics (Signal C). Each signal was added to four volumes of interest (VOIs; each with a size of 7×7×3 voxels). To simulate the noisy environment in the brain, we added random noise and structured noise [24] to the simulated data (all voxels in the brain area). To simulate random noise, we generated and added a set of four-dimensional random noise data (72×72×3×300) to the MR images. The noise follows a Gaussian distribution with a mean of 0 and a variance of 1. To simulate the structured noise, we generated a cardiac signal (Signal O), which has an average frequency of 1.1 Hz and a jitter of ±0.1 Hz. Signal O was resampled at a rate of 1.429 Hz, corresponding to a repetition time (TR) of 700 ms used in our resting-state fMRI data acquisitions. The resampled signal (Signal H) was then used to simulate the in vivo aliased cardiac signal. The magnitudes of the signals and the noises have been varied to adjust the contrast-to-noise ratio (CNR). The CNRs ranged from 0.15 to 1.5. For the same CNR, the weight of the structured noise and that of the random noise may be different. We defined K as the ratio between the magnitude of the random noise and that of the structured noise. K values ranged from 0.5 to 2.

2.2. Subjects

Ten right-handed healthy volunteers (age range, 18–45 years) with no known neurologic disorder were recruited,

trained and imaged in this study. Men and women were recruited in equal proportions through posted advertisements. Informed consent forms were obtained from each subject before any experiment started. Functional MRI scans were acquired with the subject lying supine and with the head supported by a foam-padded hemicylindrical head holder. Each subject's head was immobilized within a tightly fitting and thermally molded plastic facial mask that extended from the hairline to the chin. Each subject was asked to participate in three fMRI sessions. Only the results from the first session are reported in this article.

2.3. Task paradigm

A finger sequence movement task, in which the fingers of each subject's nondominant hand were opposed to the thumb in specific sequences, was used in our activation study [25]. During the task, the subjects were instructed to perform one of two specific sequences (Sequence A or Sequence B). In Sequence A, the order of finger movement was 4–1–3–2–4 (with the fingers numbered as follows: index finger, 1; middle finger, 2; ring finger, 3; and little finger, 4). In Sequence B, the order of finger movement was 4–2–3–1–4. Sequences A and B were matched and mirror-reversed sequences. The performances of the sequences were paced by the loud sound of the MRI scanner, with a speed of approximately two movements per second. The resting-state fMRI images were acquired before the finger sequence movement task was conducted. For the rest condition, subjects were instructed to remain motionless, to keep their eyes closed and to perform no behavioral task.

2.4. Data acquisition

The fMRI images were acquired on an Elscint Prestige 2-T whole-body MRI scanner (Elscint Prestige, Haifa, Israel). For the resting-state fMRI, seven contiguous slices were acquired in a transverse plane using a T_2*-weighted gradient-echo EPI sequence with a slice thickness of 6 mm (TR=700 ms; echo time [TE]=45 ms; flip angle (α)=70°; interslice gap=0 mm; received bandwidth=12.21 Hz). The in-plane resolution for the images was 3.28×3.28 mm^2. Four hundred seven-slice MR images were acquired. The matrix size of each slice was 72×72 voxels. Functional activation images were acquired after the resting-state studies with the use of the following parameters: 16 contiguous slices; TR=2 s; TE=45 ms; α=90°; slice thickness=6 mm; interslice gap=0 mm; and in-plane resolution=3.28×3.28 mm^2. The total number of multislice images in each run was 240. At the end of the fMRI data collection, spin-echo T_1-weighted anatomical images (TR=33 ms; TE=12 ms; α=60°; slice thickness=5 mm; interslice gap=1 mm; matrix size=256×256 voxels) in the same slice positions were acquired to facilitate the precise determination of the structures corresponding to the functional activation foci. Offline reconstruction algorithms were used to reconstruct the echo-planar images. The first 10 images of each run were discarded to allow MRI signals to reach a steady state.

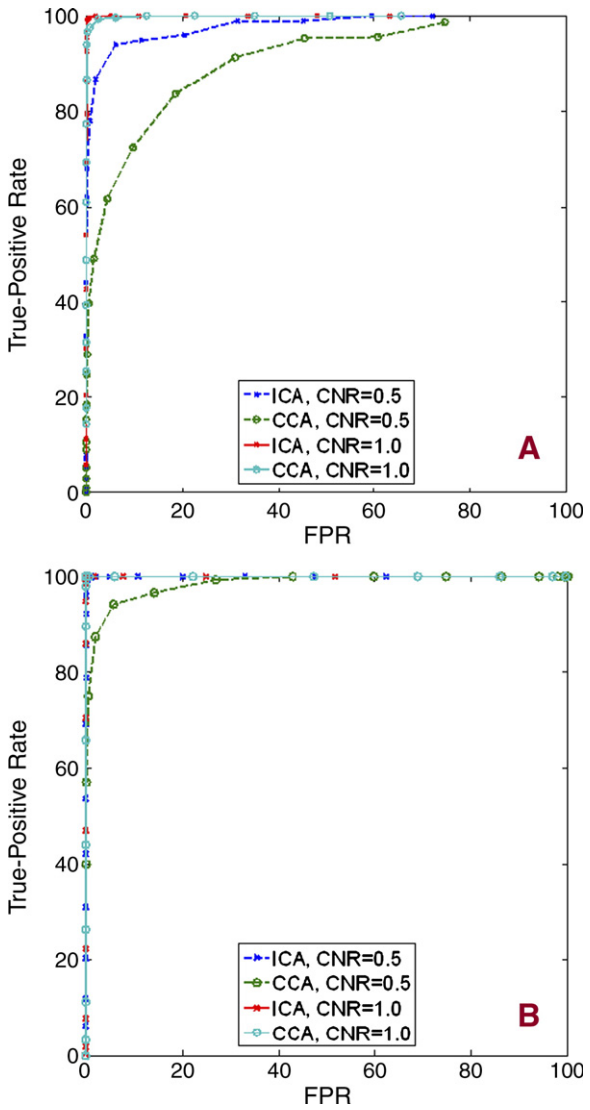

Fig. 3. ROC curves for ICA and CCA. The curves were plotted based on the average ROC curves of the three simulated signals. (A) K=2. (B) K=0.5.

2.5. Selection of seeds

For the simulated data, the simulated signals in each pair of VOIs were identical. One of the four VOIs was chosen as a volume of seeds for the CCA method. For the in vivo data, two sets of seeds (seeds I and II) were chosen for the CCA approach to investigate how the location of seeds affects the results of CCA. Seed I was chosen based on anatomical structure. Each seed consists of 7×7×3 voxels whose center was located in the right-handed primary motor cortex (M1) area. The hand M1 area lies between the superior and middle frontal gyri and is anteriorly bounded by the posterior edge of the precentral gyrus and posteriorly bounded by the anterior bank of the central sulcus [26,27]. Seed II was chosen based on the right M1

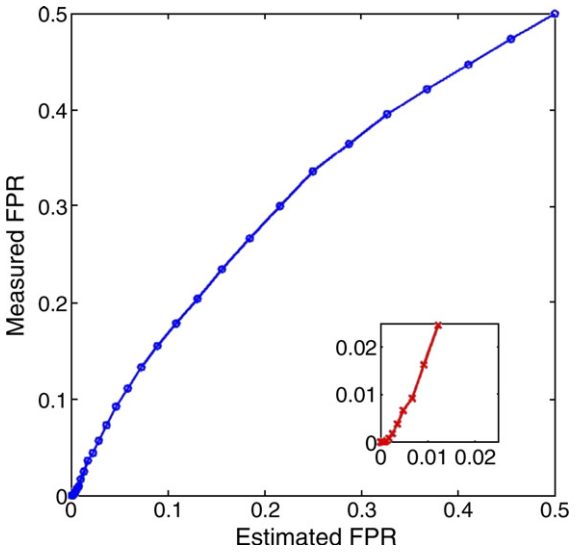

Fig. 4. The correspondence between estimated FPR and measured FPR. The curves were plotted from the simulated data under a CNR of 0.5 and a ratio of $K=2$. The subplot provides an enlarged view of the small zone close to the original point.

activations detected using the data from the finger sequence movement task. The mean of the time courses of the seed region was treated as the reference function for our resting-state CCA analysis.

2.6. Preprocessing

All in vivo fMRI images were assessed for head movement. Motion correction was performed for all data. A linear drift correction was applied to eliminate the effect of linear signal drifts. A bandpass filter with cutoff frequencies of 0.01 and 0.12 Hz was used to remove both high-frequency noise and very low-frequency signals [3,28]. To increase the signal-to-noise ratio, the data were spatially smoothened using an isotropic Gaussian filter with a full-width at half-maximum of 4.8 mm. In addition, voxels whose values exceeded 2.4 standard deviations of the time series were treated as outliers and were removed from the data [6]. The simulated data were preprocessed similarly.

2.7. Image processing

For CCA, a statistical parametric image was created for each subject by computing the correlation between each voxel and the reference function. For ICA, principal component analysis was used to reduce the dimensions of the data before ICA was applied. Different numbers of reduction were considered to study the influence of the dimensions. The range of the numbers was from 2 to 30 for both the simulated data and the in vivo data. sICA was chosen in this study and was implemented using the infomax ICA algorithm developed by Bell and Sejnowski [12]. The MATLAB (The MathWorks, Natick, MA, USA) code of the algorithm is within the electroencephalogram toolbox (CNL/Salk Institute, San Diego, CA, USA) released by Makeig et al. (http://www.cnl.salk.edu/~scott/icabib.html). The independent maps of ICA were then converted to z maps [15,20] for thresholding. A cluster of voxels was considered to be part of a functional connectivity network if it simultaneously satisfied the following conditions: (1) the intensity of each element voxel is over a specified threshold and (2) the number of voxels is over 10. Both ICA and the seed-based CCA approaches were run on a platform of MATLAB 7.0. The functional connectivity networks detected from the in vivo fMRI data were overlain onto the T_1 images of the same subject.

3. Results

The influences of noise level on the performances of ICA and CCA were first investigated using the simulated data. Fig. 2 shows the effects of noise levels on the detection of functional connectivity networks using ICA and CCA. The

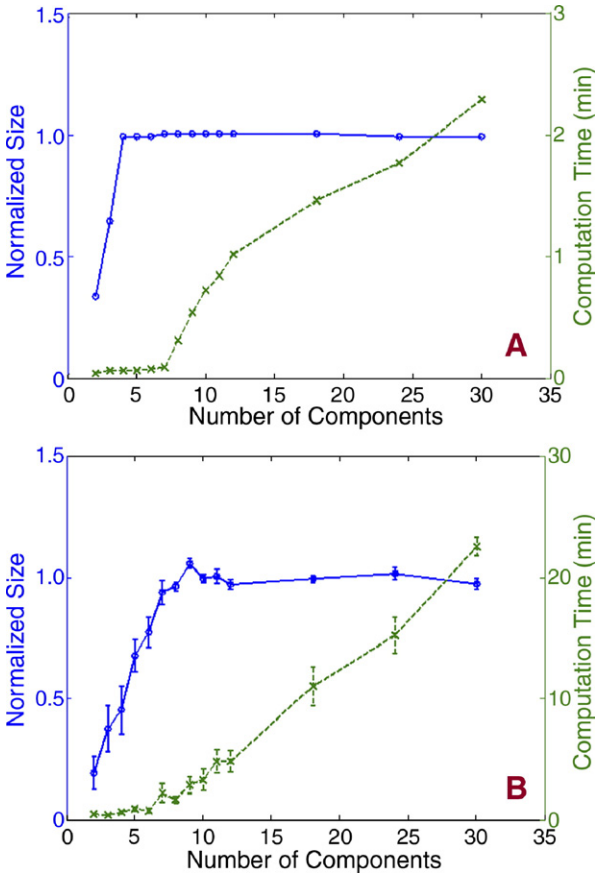

Fig. 5. The relationships between the size of the functional connectivity networks detected by ICA, the computation time and the number of ICs. (A) Functional connectivity networks obtained from the simulated data under a CNR of 0.5 and a ratio of $K=2$. The sizes were normalized by the mean value of the sizes of the last 11 points. (B) Functional connectivity networks detected from the in vivo fMRI data. The sizes were normalized by the mean value of the sizes of the last 7 points. The infomax ICA algorithm was run on a Dell desktop computer (Dell, Round Rock, TX, USA) with a Pentium 4 CPU (2.80-GHz frequency, 1 GB of RAM).

threshold was fixed at 3.5. Both ICA and CCA performed well in detecting the signals when the random noise level was low (CNR=1.0; K=0.5). When the random noise was high (CNR=0.5; K=2; Fig. 2A and E), both approaches had difficulty with detecting the interesting signals. The apparent activations shown in Fig. 2E are actually the seed regions. The most significant difference between ICA and CCA was in their capacity to deal with the structured noise (Signal H, the simulated aliased cardiac signal). Whereas the ICA approach was hardly affected by the structured noise, CCA was significantly affected by the noise. Under a high level of structured noise, CCA can detect the signals with a high true-positive rate, but the false-positive rate (FPR) was high as well.

The performances of ICA and CCA were further evaluated based on the receiving operator characteristic (ROC) curves (Fig. 3). The upper panel and the lower panel in this figure correspond to K values of 2 and 0.5, respectively. In each case, two CNRs (CNR=0.5 and CNR=1.0) were evaluated. Kolmogorov–Smirnov tests revealed a significant difference between ICA and CCA performances (P<.001) when the random noise level was high (CNR=0.5). In this situation, ICA was significantly better than CCA in detecting neuronal activity. When the random noise level was low (CNR=1.0), both ICA and CCA performed well.

The influence of converting the spatially independent maps of ICA into z maps is shown in Fig. 4, which is a scatterplot of a series of estimated FPRs versus a series of measured FPRs. The measured FPRs were obtained from Signal A (detected by ICA) under a CNR of 0.5. Based on the figure, z-map conversion tends to overestimate the FPRs. The overestimation is however not very severe and may be acceptable in most cases.

The relationship between the normalized size of the detected functional connectivity networks and the number of ICs is shown in Fig. 5. The relationship between the computation time and the number of ICs is also portrayed in the same figure. Fig. 5A was obtained from the simulation data, whereas Fig. 5B was obtained from the functional connectivity networks detected from the in vivo data. When the number of ICs was greater than the number of the source signals (e.g., four for the simulation), the results of ICA were not affected by the number. When the number of ICs was smaller than the number of the source signals, ICA results became highly dependent on the number. This

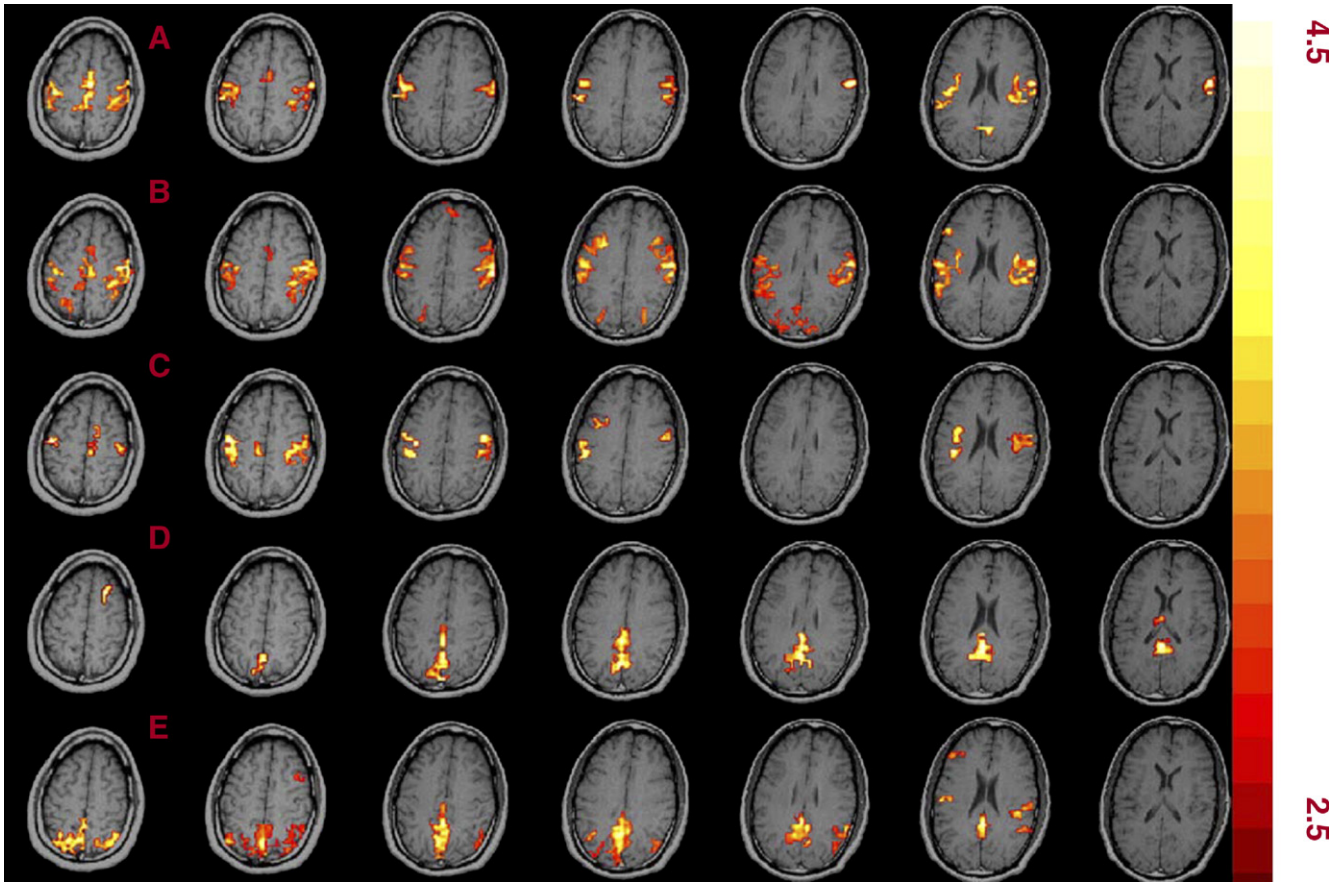

Fig. 6. The motor and visual functional networks of a single subject detected by ICA and the two seed-based CCA approaches. (A) Motor networks detected by ICA. (B) Motor networks detected by CCA seed I. (C) Motor networks detected by CCA seed II. (D) Visual networks detected by ICA. (E) Visual networks detected by CCA seed I. Because there was no functional information for the visual system study, only the results of CCA seed I are provided.

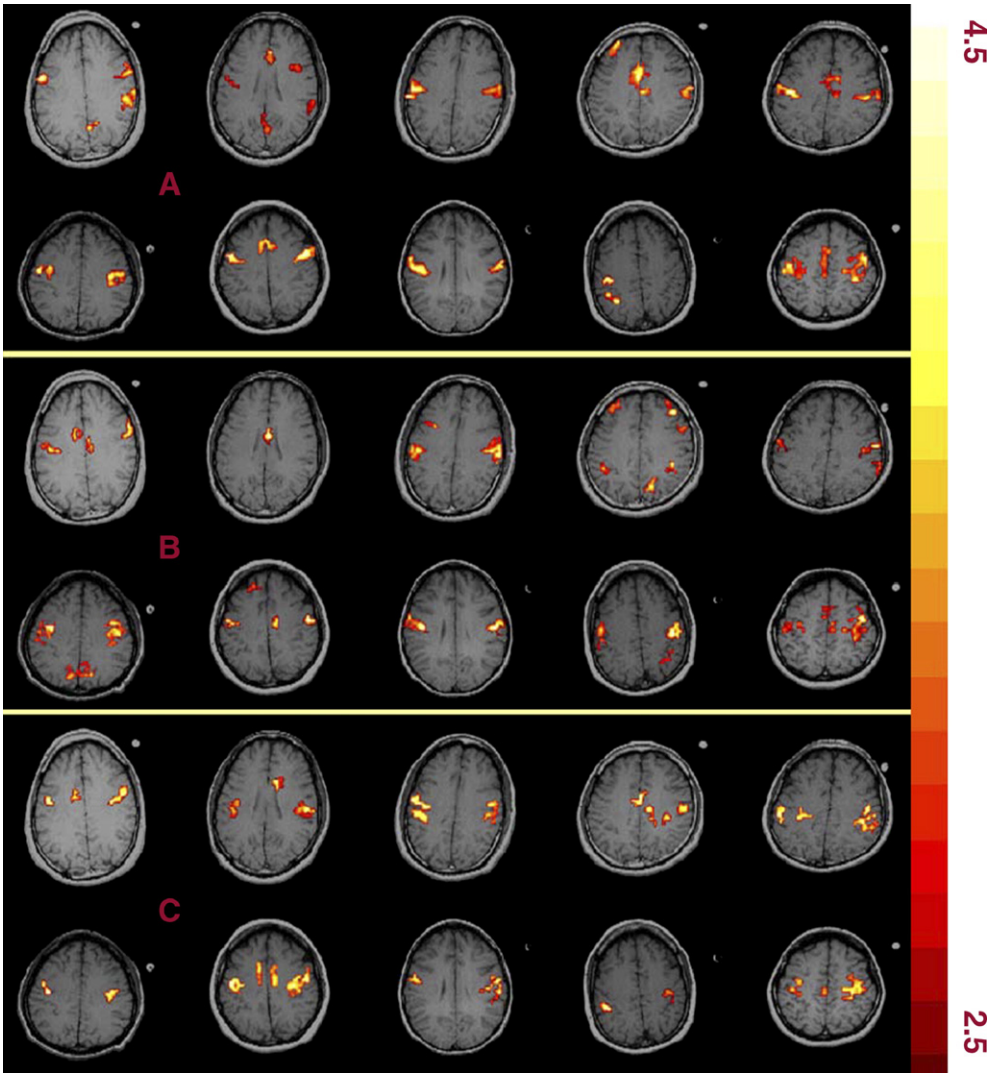

Fig. 7. The detected motor networks of the 10 subjects. (A) Motor networks detected by ICA. (B) Motor networks detected by CCA seed I. (C) Motor networks detected by CCA seed II. Only one slice is shown for each subject for the convenience of presentation.

observation also appears to be true for the in vivo fMRI data. As shown in Fig. 5B, the influence of the number was not obvious when the number was not lower than a critical value (appears to be 9 for the in vivo data in this experiment). In both cases, the computation time increased with the number of ICs. In the case of the in vivo data, the

Table 1
The sizes of the motor networks (M1s and SMA) detected by ICA and the two seed-based CCA approaches

Subject	ICA			CCA seed I			CCA seed II		
	M1 L	SMA	M1 R	M1 L	SMA	M1 R	M1 L	SMA	M1 R
1	144	110	188	37	0	85	135	0	166
2	63	48	105	108	113	91	67	48	118
3	91	74	125	151	43	171	77	31	93
4	125	15	86	54	29	74	53	42	100
5	185	67	34	32	0	112	27	30	69
6	31	85	77	0	90	124	11	15	49
7	134	162	210	144	84	185	68	54	94
8	10	57	30	11	44	29	22	19	37
9	211	101	286	390	127	393	170	38	160
10	90	29	150	228	100	265	85	0	98
Mean	108.4	74.8	129.1	115.5	63.0	152.9	71.5	27.7	98.4
SD	64.1	42.7	81.0	228.0	45.9	107.6	49.9	18.9	42.0

L = left hemisphere; R = right hemisphere.

Table 2
The locations of the motor networks (M1s) detected by the two seed-based CCA approaches

Subject	CCA seed I						CCA seed II						Distance	
	M1 L			M1 R			M1 L			M1 R				
	x	*y*	*z*	*x*	*y*	*z*	*x*	*y*	*z*	*x*	*y*	*z*	L	R
1	0.83	0.23	−1.33	1.48	−0.08	−0.17	2.29	0.32	0.19	0.12	3.55	0.01	2.11	3.88
2	0.94	3.56	−1.67	−0.54	2.56	−1.35	0.77	2.86	0.13	−2.32	2.83	0.09	1.94	2.31
3	−0.55	−1.66	0.41	1.15	−1.25	0.93	0.44	−2.64	0.11	−0.50	1.16	0.17	1.43	3.02
4	−0.36	0.15	−0.19	−0.72	0.04	−0.94	1.01	1.28	−0.05	−1.66	1.81	−0.33	1.78	2.09
5	−1.47	0.01	−2.15	−0.51	−1.63	−2.36	2.24	6.50	−2.78	−3.80	2.55	−2.65	7.50	5.33
6	4.25	−7.98	−4.09	4.65	−6.63	−1.52	0.19	−2.49	0.61	−2.14	−0.07	−0.56	8.29	7.09
7	1.12	3.56	−1.90	0.50	2.61	−1.70	0.92	2.27	0.71	−2.20	1.31	−0.53	2.92	3.22
8	−0.77	0.04	−3.00	−3.94	−6.35	−2.01	0.17	2.96	0.00	−1.12	−7.04	0.90	4.29	4.11
9	−0.20	−3.41	1.30	0.34	−1.37	0.31	1.13	−0.84	0.62	−0.72	−0.76	−0.20	2.97	1.33
10	−0.53	−1.48	1.37	−0.06	−2.62	0.72	0.88	0.76	1.06	−2.06	1.59	−0.47	2.66	4.81
Mean	0.33	−0.70	−1.13	−0.70	−1.47	−0.89	1.00	1.01	0.06	−1.64	0.69	−0.38	3.59	3.71
SD	1.61	3.35	1.81	2.03	3.14	1.18	0.74	2.76	1.06	1.12	3.01	0.92	2.41	1.71

The *x*-, *y*- and z-coordinates are relative values (to those detected by ICA). The distance is the Euclidean distance between the centers of motor networks detected by CCA seed I and CCA seed II.

computation time increased exponentially with the number of ICs.

The performances of ICA and CCA were also evaluated using the in vivo resting-state fMRI data. Fig. 6 shows the motor and visual networks detected by ICA, CCA seed I and CCA seed II for a single subject. For all the three methods, significant functional connectivity networks were detected in the motor and visual systems. For the motor system, the detected regions were M1, primary somatosensory cortex, supplementary motor area (SMA), dorsal premotor cortex, posterior parietal somatosensory association area and dorsal cingulate motor area. All the detected areas are known to be closely related to the M1. For the visual system, predominant activity was localized in the primary and the secondary visual areas.

Fig. 7 shows the motor functional connectivity networks of the 10 individual subjects as detected by ICA, CCA seed I and CCA seed II. The results show that all the three approaches were able to detect the functional connectivity network of the motor system. Consistency was fairly good across the different subjects.

The sizes of the motor system (left M1, SMA and right M1) detected by ICA and the two CCA approaches are summarized in Table 1. A two-factorial analysis of variance was performed to test differences between different analytical approaches (ICA and the two CCA methods) and different brain regions of the motor connectivity networks. Our tests revealed significant differences among the three approaches ($F_{2,81}=3.46$; $P<.05$) and the three brain regions ($F_{2,81}=7.74$; $P<.05$) but failed to detect significant differences in interaction ($F_{4,81}=0.16$; $P>.05$). Tukey's HSD post hoc test showed that the CCA approach depends on the position of the seeds ($P<.05$).

Table 2 shows the relative location (represented by *x*, *y*, *z* and Euclidean distance) between centers of the M1 connectivity networks as detected by the two seed-based CCA approaches. Student's *t* test based on the Euclidean distances revealed that the relative Euclidean distances of the M1 networks detected by the two seed-based CCA approaches are significantly different ($t=4.70$ and $P<.05$ for the left M1; $t=6.88$ and $P<.05$ for the right M1). Again, our test findings indicate that CCA results depend on the position of the seed.

4. Discussion and conclusion

ICA and CCA are both capable of detecting resting-state functional connectivity networks. However, the performances of ICA and CCA are not necessarily always the same. ICA significantly differs from CCA in terms of the size and location of the detected networks. Importantly, ICA significantly differs from CCA in overall performance and in handling aliased cardiac signals. Based on our results, the overall performance of ICA appears to be significantly better than that of CCA for resting-state fMRI data analysis.

Functional MRI data are typically contaminated by both structured noise (cardiac and respiration) and unstructured noise (white noise) [24]. Although a relatively low sampling rate (1.429 Hz) was used in our experiment, aliased cardiac signal still presented in our fMRI data. Our results indicate that the performance of ICA is superior to that of CCA when the structured noise is strong. The performance of ICA is mainly affected by random noise and is hardly affected by structured noise. This bestows ICA an ability for noise reduction, as also reported by Thomas et al. [24]. In contrast, the performance of CCA depends on both random and structured noises. The detected networks are very noisy if the structured noise is strong (Fig. 2F and H). ICA can be performed by maximizing statistical independence either spatially or temporally (sICA vs. tICA). In our study, sICA was used for analyzing fMRI data. By driving the spatial components as independently as possible, sICA was not optimized to separate temporally mixed signals. As shown in Fig. 2, ICA is capable of detecting all signals

simultaneously. However, the time courses for each spatial map are similar but not temporally independent. As for CCA, it works in time domains and manages to explore the temporal feature of the data differently. It however requires three seeds (seeded on Signals A–C) to completely detect the three artificial signals. This difference between ICA and CCA may bear profound effects on in vivo fMRI experiments. Let us consider a simple example: Assuming three subsystems A, B and C, subsystems A and B are temporally independent and subsystem C is under the influence of subsystems A and B. Depending on the location of seeds, CCA may detect brain subsystem A, B or C only (seeded on A, B or C); that is, CCA results are strongly affected by the seed location and may only detect partial systems. In contrast, ICA will detect all three subsystems A, B and C simultaneously. The three brain regions will however most likely be presented as three separate maps. A complete connectivity network could be obtained by combining the three maps. In actual functional neuroimaging studies, how to combine or whether to combine the individual maps is a difficult decision to make if no prior knowledge is available.

One problem of ICA is that it is difficult to associate thresholds with significant levels for ICA. As a technique of blind source separation, ICA separates signals by minimizing the statistical dependence among the separated signals, which are assumed to be non-Gaussian. Since the amplitude of a separated signal is arbitrary, it is theoretically difficult to assess the statistically significant level of the ICA map. In practice, a z-map conversion is proposed to convert an independent map with a non-Gaussian distribution into a z map with a Gaussian distribution [15,20]. The significant level can then be assigned based on the z map. Is this conversion applicable? In this study, we evaluated the effect of z-map conversion by investigating the consistency between the measured FPRs and the estimated FPRs. Our results show that the z-map conversion tends to overestimate the FPRs. The overestimation is however not very severe and may be acceptable in most cases.

Since the first application to fMRI analysis, how to determine the optimal number of ICs has become an open problem in ICA. Some researchers suggested that the data should not be compressed too much (e.g., keeping 99% of the contents of the original data) to avoid losing important information, resulting in a very large number of ICs (e.g., 144 components) [15]. Since the number of source signals (e.g., the brain dynamics, cardiac, respiration, head movement and other artifacts) is usually not very high in fMRI data, many signals with a Gaussian distribution (e.g., random noise) will appear as separated signals if too many ICs are used. This violates one of the basic assumptions in ICA, which assumes no more than one source signal following a Gaussian distribution [13]. In addition, our experiments show that the computation time increases exponentially with the number of ICs. Theoretically, the optimal number of ICs can be estimated using Akaike's information criterion and/or minimum description length [29]. These approaches however suffer from the difficulty of determining the minimum of the information criterion, which is often not unique. In our study, we estimated the number of ICs experimentally. Our results demonstrate that MRI data can be compressed more significantly without preventing ICA from extracting interesting maps. When the number of ICs is equal to or greater than the number of source signals, the influence of the number of ICs is insignificant. ICA results are affected by the number of ICs only when the number is smaller than the number of source signals. In that case, the size of the detected functional connectivity networks significantly decreases with a decrease in the number of ICs. In our experiment, this critical value is 3 for the simulated data and appears to be 9 for the in vivo fMRI data. Our results are consistent with those of Zhao et al. [20], who reported that the number of ICs can be as low as 10.

The effect of seeds on connectivity maps is a great concern for resting-state fMRI data analyses using CCA. Different techniques have been used to select seeds location. Our experimental results show that CCA is seeds sensitive. Seeds based on different criteria create significant differences in the size and location of connectivity networks. As no single technique is accepted as standard, flexibility in seeds selection will inevitably introduce additional variability in resting-state connectivity maps across different laboratories.

In summary, ICA and CCA are capable of detecting resting-state functional connectivity networks. However, ICA significantly differs from CCA in terms of the size and location of the detected networks. It is an automatic method and can detect different kinds of functional connectivity networks simultaneously. The z-map conversion of ICA tends to overestimate the FPR, but not very severely. In addition, the results of ICA are influenced by the number of the independent maps if this number is too small. The influence becomes nonobvious when the number of ICs is greater than a critical value. On the other hand, CCA results are dependent on seeds location; different seeds may result in different detections. Based on our ROC curve analysis, the overall performance of ICA is better than that of CCA. Furthermore, its robustness to structured noise renders ICA another advantage over CCA.

Acknowledgment

This work was financially supported by the NSF (Grant No. BCS 05-09626) and the NIH (Grant No. 5 RO1 NS046082).

References

[1] Biswal BB, Yetkin FZ, Haughton VM, Hyde JS. Functional connectivity in the motor cortex of resting human brain using echo-planar MRI. Magn Reson Med 1995;34:537–41.

[2] Xiong J, Parsons LM, Gao J-H, Fox PT. Interregional connectivity to primary motor cortex revealed using MRI resting state images. Hum Brain Mapp 1999;8:151–6.
[3] Cordes D, Haughton VM, Arfanakis K, Carew JD, Turski PA, Moritz CH, et al. Frequencies contributing to functional connectivity in the cerebral cortex in "resting-state" data. AJNR Am J Neuroradiol 2001; 22:1326–33.
[4] Lowe MJ, Mock BJ, Sorenson JA. Functional connectivity in single multislice echoplanar imaging using resting-state fluctuations. Neuroimage 1998;7:119–32.
[5] Biswal BB, Yetkin FZ, Haughton VM, Hyde JS. Functional connectivity in the auditory cortex studied with fMRI. Neuroimage 1996;3:305.
[6] Hampson M, Peterson BS, Skudlarski P, Gatenby JC, Gore JC. Detection of functional connectivity using temporal correlations in MR images. Hum Brain Mapp 2002;15:247–62.
[7] Kiviniemi V, Kantola J-H, Jauhiainen J, Hyvärinen A, Tervonen O. Independent component analysis of nondeterministic fMRI signal sources. Neuroimage 2003;19:253–60.
[8] Quigley MA, Cordes D, Turski P, Moritz C, Haughton V, Seth R, et al. Role of the corpus callosum in functional connectivity. AJNR Am J Neuroradiol 2003;24:208–12.
[9] Matsumoto R, Nair DR, LaPresto E, Najm I, Bingaman M, Shibasaki H, et al. Functional connectivity in the human language system: a cortico-cortical evoked potential study. Brain 2004;127:2316–30.
[10] Stein T, Moritz C, Quigley M, Cordes D, Haughton V, Meyerand E. Functional connectivity in the thalamus and hippocampus studied with functional MR imaging. AJNR Am J Neuroradiol 2001;21:1397–401.
[11] He Y, Zhang Y, Jiang T, Liang M, Gong G. Detecting functional connectivity of the cerebellum using low frequency fluctuations (LFFs). Medical Image Computing and Computer-Assisted Intervention—MICCAI. LNCS 2004;3217:907–15.
[12] Bell AJ, Sejnowski TJ. An information-maximization approach to blind separation and blind deconvolution. Neural Comput 1995;7: 1004–34.
[13] Hyvärinen A, Karhunen J, Oja E. Independent component analysis. John Wiley and Sons, 2001.
[14] Calhoun VD, Adali T, Hansen LK, Larsen J, Pekar JJ. ICA of functional MRI data: an overview. Fourth International Symposium on Independent Component Analysis and Blind Signal Separation (ICA2003). Japan: April, Nara; 2003. p. 281–8.
[15] McKeown MJ, Makeig S, Brown GG, Jung T-P, Kindermann SS, Bell AJ, et al. Analysis of fMRI data by blind separation into independent spatial components. Hum Brain Mapp 1998;6:160–88.
[16] McKeown MJ, Hansen LK, Sejnowski TJ. Independent component analysis of functional MRI: what is signal and what is noise? Curr Opin Neurobiol 2003;13:620–9.
[17] Calhoun VD, Adali T, Pearlson GD, Pekar JJ. Spatial and temporal independent component analysis of functional MRI data containing a pair of task-related waveforms. Hum Brain Mapp 2001; 13:43–53.
[18] Biswal BB, Ulmer JL. Blind source separation of multiple signal sources of fMRI data sets using independent component analysis. J Comput Assist Tomogr 1999;23:265–71.
[19] Quigley MA, Haughton V, Carew J, Cordes D, Moritz C, Meyerand ME. Comparison of independent component analysis and conventional hypothesis-driven analysis for clinical functional MR image processing. AJNR Am J Neuroradiol 2002;23:49–58.
[20] Zhao X, Glahn D, Tan LH, Li N, Xiong J, Gao J-H. Comparison of TCA and ICA techniques in fMRI data processing. J Magn Reson Imaging 1999;19:397–402.
[21] Yang K, Rajapakse JC. ICA gives higher-order functional connectivity of brain. Neural Inf Process Lett Rev 2004;2:27–32.
[22] van de Ven VG, Formisano E, Prvulovic D, Roeder CH, Linden DEJ. Functional connectivity as revealed by spatial independent component analysis of fMRI measurements during rest. Hum Brain Mapp 2004; 22:165–78.
[23] Beckmann CF, DeLuca M, Devlin JT, Smith SM. Investigations into resting-state connectivity using independent component analysis for functional magnetic resonance imaging. Philos Trans R Soc B 2005; 360:1001–13.
[24] Thomas CG, Harshman RA, Menon RS. Noise reduction in BOLD-based fMRI using component analysis. Neuroimage 2002;17:1521–37.
[25] Karni A, Meyer G, Jezzard P, Adams MM, Turner R, Ungerleider LG. Functional MRI evidence for adult motor cortex plasticity during motor skill learning. Nature 1995;377:155–8.
[26] Solodkin A, Hlustik P, Chen EE, Small SL. Fine modulation in network activation during motor execution and motor imagery. Cereb Cortex 2004;14:1246–55.
[27] Boling W, Olivier A, Bittar RG, Reutens D. Localization of hand motor activation in Broca's pli de passage moyen. J Neurosurg 1999; 91:903–10.
[28] Beckmann CF, Smith SM. Probabilistic independent component analysis for functional magnetic resonance imaging. IEEE Trans Med Imaging 2004;23:137–52.
[29] Calhoun VD, Adali T, Pearlson GD, Pekar JJ. A method for making group inferences from functional MRI data using independent component analysis. Hum Brain Mapp 2001;14:140–51.